Techno-Science Research Journal 11(2) (2023) 57-67

Content list available at ITC

Techno-Science Research Journal

Journal Homepage: http://techno-srj.itc.edu.kh/

Techno-Science Research Journal

Non-intrusive Load Monitoring Classification Based on Multi-Scale Electrical Appliance Load Signature

Manith Chou[1*], Kosorl Thourn[2]

[1] *Mechatronics, Information and Communication Technology Reseaech Unit, Research and Innovation Center, Institute of Technology of Cambodia, Russian Federation Blvd., P.O. Box 86, Phnom Penh, Cambodia*

[2] *Department of Telecommunication and Network Engineering, Institute of Technology of Cambodia, Russian Federation Blvd., P.O. Box 86, Phnom Penh, Cambodia*

Received: 07 June 2023; Accepted: 07 October 2023; Available online: December 2023

Abstract: *Non-intrusive load monitoring systems (NILM) have attracted much attention due to their potential contribution to energy savings for individual households. The approach analyzes the load consumption of each device in terms of the total energy consumption of the house. The selection of essential load signatures for load identification expresses a crucial challenge with NILM techniques. Several studies that have been proposed in the literature claim that the Voltage and Current (V-I) trajectory has identified the most effective individual steady-state signature for appliance identification. In addition, multi-scale approaches utilized to derive the load signature have limitations. Therefore, this study is focused on one cycle of steady-state voltage and current used to generate a voltage-current trajectory. Next, the Fourier phase correction approach has been employed to eliminate the issue of current and voltage starting points. Afterward, the corrected starting point of the V-I trajectory of each electrical load appliance is then represented by the Triangle Area Representation (TAR) at various side lengths. Since the TAR signature contains an extremely high-dimensional subspace, it is significant to perform Principal Component Analysis (PCA) to produce a low-dimensional space feature. Consequently, appliance identification has been improved based on the weighted K-nearest neighbor (W-KNN) multi-classification technique. In addition, the Plug Load Appliance Identification Dataset (PLAID) with three different versions is used to evaluate the performance of the proposed algorithm. As a result, our proposed algorithm with these datasets improves accuracy results compared to state-of-the-art approaches that relied on steady-state signatures for load identification.*

Keywords: Non-intrusive Load Monitoring; V-I trajectory; Multi-Scale Signature; Triangle Area Representation, Principal Component Analysis, Weigted K-nearest Neigbors

1. INTRODUCTION

Growth in electrical consumption has increased significantly. Electrical power has become an essential part of modern social development. As demand rises, issues such as an energy crisis, climate change, and energy conservation will emerge, affecting the country's overall economy. Due to the numerous network connections of electrical appliances and technological equipment, power consumption has also significantly increased faster than global population growth. According to the United States Energy Information Administration (EIA), in 2000, global electricity net consumption was 13,277 billion kilowatt-hours (kWh), a number that increased to 22,347 billion kWh in 2017 [1].

In recent years, energy management has become a sensitive topic that requires the monitoring and control of electrical utilities to save energy or reduce energy consumption [2]. Advanced Metering Infrastructure (AMI) is a term for systems that measure, collect, and analyze energy use and communicate through metering devices. Load monitoring is an element of AMI that breaks down aggregated energy consumption data into the power consumption of individual devices and analyzes relevant power data that can be used to manage energy, save energy, diagnose device faults, and respond to power demand [3]. According to the research, when consumers receive an electrical bill that includes specific information on the energy use of individual appliances, they could save up to 12% [4,5]. Electricity consumption in Cambodia reached 11.5 terawatt-hours in 2020 [5]. Based on a 12% savings if consumers receive specific information on their energy usage, this ratio could represent 1.38 terawatt hours per year in energy savings.

Appliance load monitoring techniques are separated into

* Corresponding author: Manith Chou

E-mail: manith_chou@gsc.itc.edu.kh; Tel: +855-98 370 065

two categories, namely the Intrusive Load Monitoring method (ILM) and the Non-intrusive Load Monitoring method (NILM), which are used in identifying appliances based on power consumption. ILM installs sensors in each device to measure energy consumption. Although it can perform high-precision monitoring, it also results in high installation costs [6]. In response to the limitations of the direct sensing approach, Non-Intrusive Load Monitoring (NILM), first introduced by Hart [7], relies only on single-point measurements of voltage and current. The NILM techniques analyze the input voltage and current of total electricity consumption and monitor appliance utilization using feature extraction and load identification algorithms. In addition, it can be widely used in various fields and has the advantages of low installation costs, minimal user intervention, and flexible use [8].

A load device or appliance has a distinctive electrical expression considered a load signature. The NILM method extracts features for load identification from various load signatures. Hart [7] first proposed the usage of the version of power as load features. After that, power load signatures have been used in numerous studies on NILM, which separates individual loads from an aggregate signal [9, 10]. Nevertheless, for appliances with similar power usage, the identification accuracy will be significantly reduced. Load signatures can be recognized by extracting information from input current and voltage signals during transient and steady-state processes on the appliance.

Transient approaches utilize the characteristics of the state transitions of a load device. For instance, wavelet transform [11], S-transform [12], transient power, and start-up current [13] are features obtained in a transient state. The use of transient signatures can improve the accuracy of load recognition. In addition, the extraction of transient load signatures requires a high sampling frequency and large data storage. Furthermore, these techniques would not differentiate between appliances with similar transient characteristics [14]. On the other hand, Steady-state methods truncate a steady-state signal from raw data such as odd-even harmonic ratio, active power, reactive power, and apparent power [15]. In addition, Mulinari et al. [16] have proposed eight different features from the V-I trajectory [17] in terms of steady state and transient region.

Many techniques based on steady-state and transient features have been proposed in the literature. Voltage-Current (V-I) trajectories can be identified among various approaches, particularly in steady-state regimes. V-I trajectories are essential as load signatures for NILM algorithms, as they can integrate several features from the interaction between the current and voltage waveforms of appliances. Numerous scalar load signatures have been derived through this kind of signature [16, 17, 18, 19].

Thus far, there seems to be little study of the multi-scale approach used in the NILM technique, which means these approaches utilized to derive the load signature have limitations. Numerous shape-based signatures can be discovered in the field of image processing, and it has been proposed that a multi-resolution shape signature approach can increase shape classification performance [20]. Furthermore, the resulting Multi-scale TAR (MTAR) is more noise-resistant, less complicated, and more selective than related approaches such as curvature scale-space (CSS) [21].

Additionally, image-based V-I or multi-scale features are represented by 2D matrices in a high-dimensional space. It would require extensive computational resources for identification. A dimensionality reduction technique can be used in order to reduce this complexity. For instance, Principal Component Analysis (PCA) is a statistical approach used to reduce the dimensionality of data [22, 23]. Moreover, [24, 25, 26] demonstrates the various implementations of PCA in the NILM methodology. Gao et al. [24] use PCA to reduce the dimension of various features, such as raw current, quantized features, and VI binary images. The principal component analysis (PCA) is used in the NILM classification system to reduce the dimension of NILM power features in order to improve real-time NILM classification [25], and it is used to extract valuable features from power consumption data in order to detect consumer type by presenting high-dimensional data in a low-dimensional space while retaining as much information from the initial data as possible [26].

In this context, the primary objective of this study is to enhance the accuracy of load identification within the NILM classification framework. The study aims to accurately identify and differentiate between different appliance types by employing an efficient load signature, advanced feature extraction, and classification techniques that effectively address the challenge of overlapping energy consumption patterns. This work introduces a novel multi-resolution technique called Triangle Area Representation (TAR) for NILM classification. This proposed signature is directly computed from the V-I trajectory in the steady-state region. The TAR signature is then applied to PCA in order to generate a low-dimensional space feature with only the most essential components. To evaluate the performance of the algorithm, a publicly available dataset (PLAID) is used, and load classification is done with a machine learning algorithm (W-KNN).

The rest of this paper is organized as follows. Section II presents the previous features addressed in the literature, which are based on the V-I trajectory. Section III introduces the methodology, which includes pre-processing, feature extraction, and classification. Section IV illustrates the results of our load classification. Finally, the conclusions and future works are provided in Section V.

1. RELATED WORK

This section provides an overview of the existing research on how they extracted the feature through the V-I trajectory. The V-I trajectory is the mutual locus of the steady-state instantaneous voltage and current. Using the normalized values of I and V during one cycle, the plot gives different shapes depending on the load connected. According to previous research, V-I trajectories have been used with various techniques to represent a feature of the load signature. These various techniques can be divided into the scarlar shape-based signature, the image-based signature, and a novel multi-sale approach called the culvature scale space signature. The following subsections will provide additional explanations of each of these techniques, providing a thorough understanding of their respective methodologies and approaches.

2.1 Shape-based V-I trajectory

Scalar shape-based signature techniques characterize load signatures by utilizing the distinct shapes formed by the V-I trajectory, providing valuable insights into the underlying load behavior. Lam et al. [17] are the first group to develop a taxonomy of a 2-dimensional form of load signatures based on the shape of the voltage and current trajectory obtained using one cycle of the voltage (horizontal axis) and current (vertical axis) at a steady state of a load. This literature proposes a few shape-based features connected to the physical characteristics of a load, such as:

- *Asymmetry:* A V-I trajectory with asymmetry is presented by one load with different shape and peak current in the positive and negative cycles.
- *Area:* The difference between the phases of the current and the voltage determines this feature.
- *Area of left and right segments:* This feature shows the phase difference between the appliance's peak current and voltage.
- *Culvature of mean line:* Similar to harmonic distortion, this feature is used to describe the distortion of a mean-line appliance's non-linearity.
- *Looping direction:* The phase angle between the voltage and current is connected to the looping direction of a trajectory. The direction of the trajectory's points is clockwise if the phase angle is positive. If not, the phase angle is negative.
- *Peak of middle segment:* The maximum peak of a trajectory's middle segment is measured. Small power consumption loads typically have a significant peak in the middle segment.
- *Slop of middle segment:* The slope of the middle segment of the trajectory is near to zero due to the conduction characteristic of specific components in electrical equipment.
- *Self-intersection:* The number of self-intersections for a V-I trajectory is proportional to the number of higher-order harmonics in the current waveform.

Afterward, Wang et al. [19] discuss a possible quantification and formalization of the previously mentioned features, as well as the addition of two new steady-state features:

- *Current span:* is referred to as the active power magnitude of the load appliance, denoted as *itc*.
- *Variation of instantaneous admittance:* This feature distinguishes between non-resistive and resistive loads. The admittance standard deviation is added to the features, denominated as *D*.

Recently, the 2D shape descriptor technique and another technique are applied to extract the one cycle in the steady-state region [27], which is determined as:

- *Convex Hull Area:* The convex hull area of the non-linear appliance is always larger than that of the resistive load appliance. The objective is to determine the area between the convex hull and the trajectory.
- *Trajectory's Length or Steady-State Current Span:* This feature is used to present the current magnitude in the steady-state area,which is linked to the horizontal length of the trajectory prior to normalization.

2.2 Image-based V-I representation

In contrast to the scalar shape-based method, image-based signature techniques transform the V-I trajectory into visual representations [24, 28, 29, 30], allowing the use of image processing and computer vision methods to extract useful features from the load signatures. The original V-I trajectory is transformed into a grid of cells with the colors black and white [24, 25] to create the binary V-I trajectory. According to Gao et al. [24], the amplitude-normalized Voltage-Current (VI) trajectories are transformed into binary pictures by creating a mesh on the original VI trajectories and making each cell 1 if it contains points and 0 otherwise. Moreover, Du et al. [28] show the algorithm for mapping V-I trajectory to cell grids with binary values.

Since it is not simple to extract characteristics from the VI trajectory, instead, by meshing the VI trajectory, the VI trajectory may be transformed into a pixelated VI picture (n x n matrix). To completely use the information contained in the VI trajectory, De Baets et al. [29] propose representing it as a weighted pixelated image with continuous values rather than binary values.

2.3 Culvature scale space signature

The curvature-scale space signature is a novel method that offers a multi-scale analysis of the V-I trajectory curvature to capture further details and variations in load behavior. To enhance the image-based V-I representation in NILM classification, de Paula Rodrigues and da Silveira [31] propose extracting two bidimensional steady-state load signatures from the curvature scale space of voltage-current trajectories. These signatures aim to improve the discriminative characteristics of image-based V-I representations. However, existing methods often overlook the phase delay between current and voltage waveforms, which contains valuable information for load identification. The proposed curvature scale space-based signatures are derived from the curvature function, which measures the displacement between the parametric components of a planar shape. The first signature, ECSS, combines the image-based V-I representation with the extrema points detected on each curvature function obtained during the process. The second signature, DCSS, is constructed by progressively smoothing the components of a closed planar curve using a Gaussian kernel with varying standard deviation. This results in a continuously increasing sequence of scale values that generates representations of closed planar curves. Experimental evaluation demonstrates promising results, with the curvature scale space-based signatures outperforming traditional methods in load classification accuracy, particularly in scenarios where phase delay significantly influences the classification outcomes.

2. METHODOLOGY

In this work, the methodology is organized into three main sections: preprocessing, feature extraction, and classification, in order to classify each type of appliance. The overall framework of the proposed algorithm is illustrated in Fig. 1.

3.1 Data preprocessing

In this stage, the raw current and voltage signals of each electrical load appliance are utilized in this approach. The V-I trajectory of each appliance is extracted by truncating the steady-state voltage and current waveforms. In a steady-state region, only one cycle is extracted and denoted by the vectors $V(t)$ and $I(t)$ for voltage and current, respectively. In order to reduce computational resources, these vectors are downsampled two times, and denoted as $S_1, S_2, S_3, \ldots, S_M$, where $S_i = (V_i, I_i)$, and $i = (1, 2, 3, \ldots, M)$.

Next, after obtaining the reduced data, Fig. 2 is examined, revealing disparate starting points for each appliance, making it challenging to identify the load signature of the V-I trajectory. The marker on each trajectory represents the starting point of the sampled signal. It can be assumed that the different starting point of the sampled signal will result in low accuracy or misclassification. To eliminate this issue, the Fourier phase correction approach has been employed [32].

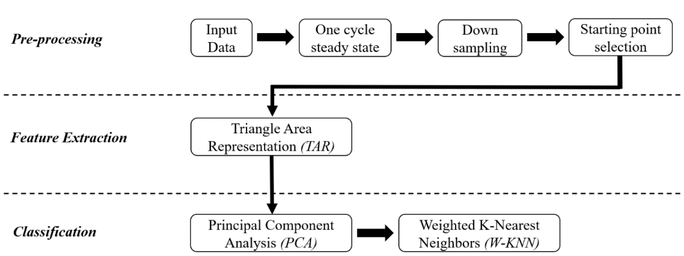

Fig. 1. The diagram of the proposed algorithm in the methodology process.

The phase correction technique has been used to determine the starting point dependency. The process of this method is that the current signal in the time domain is transformed into the frequency domain by using the Discrete Fourier Transform (DFT). The sequence of the current signal $I(1), I(2), \ldots\ldots, I(M)$ is converted to a new sequence according to the formula of DFT:

$$\tilde{I}(i) = R_i \exp(j\theta_i) \qquad i = 1,2,3,\ldots\ldots,M \qquad \text{(Eq. 1)}$$

In the frequency domain, its magnitude and phase are computed. Subsequently, the phase is corrected to be invariant to the starting point. The DFT coefficients $\hat{I}(i) = \hat{R}_i \exp(j\hat{\theta}_i)$ are normalized following the equation below:

$$\hat{\theta}_i = \theta_i - i\frac{\theta_{-1}+\theta_1}{2} \qquad \text{(Eq. 2)}$$

Using inverse DFT, new samples of the current signal with magnitude and corrected phase can be obtained. Next, the voltage signal $\hat{V}(i)$ is adjusted without the use of DFT by simply rearranging the sampled points of the voltage signal to correspond with those of the new current signal.

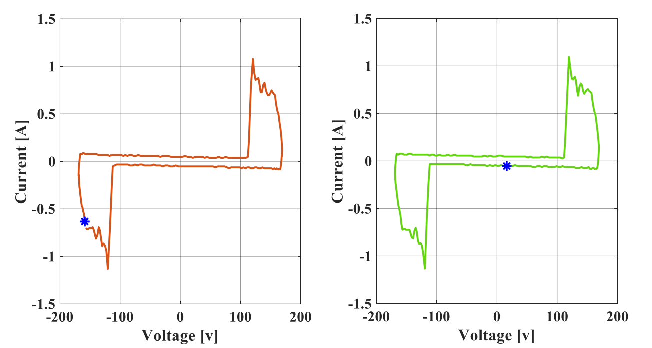

Fig. 2. The V-I trajectories of two load appliances of Compact fluorescent lamp.

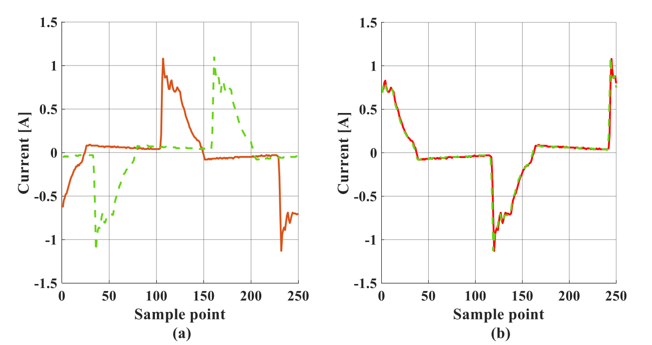

Fig. 3. The extracted steady-state current of two Compact fluorescent lamps for one cycle (a) before and (b) after applying Fourier phase correction approach.

As depicted in Fig. 3(b), after using the phase correction technique, both current waveforms corresponding to two compact fluorescent lamps look very similar, whereas the signals are mismatched before correcting the phase, as shown in Fig. 3(a).

Finally, the center of mass of the trajectory is shifted to the origin. It can be determined as follows:

$$\begin{cases} \bar{V}_i = \hat{V}_i - V_m \\ \bar{I}_i = \hat{I}_i - I_m \end{cases} \quad \text{(Eq. 3)}$$

where $V_m = \frac{1}{N}\sum_{i=1}^{N} V_i$ is the center of mass of V_i, and $I_m = \frac{1}{N}\sum_{i=1}^{N} I_i$ is the center of mass of I_i

3.2 Feature extraction

Feature extraction plays an important role in the study of load signatures. After the voltage and current signals are normalized in the preprocessing step, the features of each appliance need to be extracted to identify their unique characteristics. A multi-scale technique called the triangle area representation is adopted to extract the appliance signature [33].

The area of a triangle, which is generated by any three consecutive sampled points on the V-I trajectory. $(\tilde{V}_{i-l}, \tilde{I}_{i-l})$, $(\tilde{V}_i, \tilde{I}_i)$ and $(\tilde{V}_{i+l}, \tilde{I}_{i+l})$, is computed to provide the triangle area representation (TAR) signature with various triangle side lengths (TSL). Fig. 4 provides a visual representation of the area of the triangle represented on the V-I trajectory with consecutive sampled points. For instance, the red curve is the V-I trajectory of Fan, and the blue line is the area of the triangle at the first sample point at the triangle side length equal to 70. This TAR signature is represented by a two-dimensional (2D) matrix, which is also plotted in 3D format as shown in Fig. 5, with the z-axis presenting the normalized value of the TAR for each sample point and TSL. Following the expression in (Eq. 4), TAR can be computed.

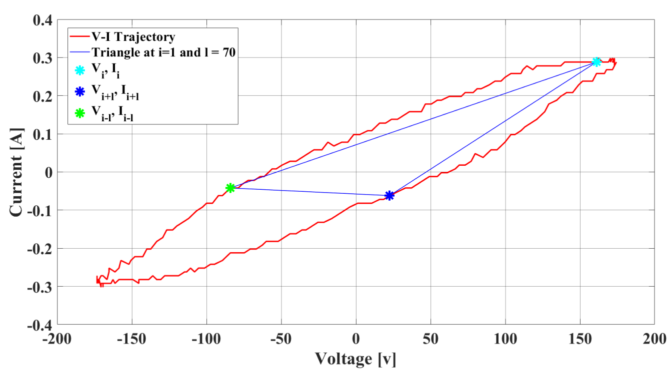

Fig. 4. The form of the area of the triangle represented on the V-I trajectory.

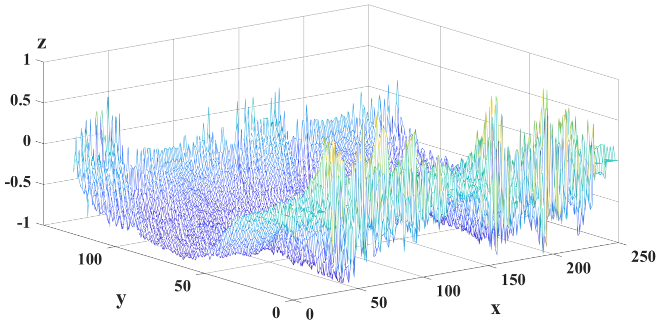

Fig. 5. TAR at different TSL of Fan . x is the sampled point index, y is the level of TSL, and z is the normalized value of TAR signature.

$$TAR(i,l) = \frac{1}{2}\begin{vmatrix} \bar{V}_{i-l} & \bar{I}_{i-l} & 1 \\ \bar{V}_i & \bar{I}_i & 1 \\ \bar{V}_{i+l} & \bar{I}_{i+l} & 1 \end{vmatrix} \quad \text{(Eq. 4)}$$

where l = 1, 2, 3 …, ⌊ N−1/2 ⌋ is a number of TSL.

3.3 Classification process

As described in feature extraction, the shape of V-I trajectories can be extracted using the TAR method. Specifically, the shape features are represented in 2D matrices, where each row corresponds to TAR at each sampling point and each column corresponds to levels of triangle side length. To prepare data for classification, 2D matrice is transformed into a single-column feature vector by concatenating the order of their rows. Containing such feature vectors with a very high-dimensional subspace, this work demonstrates the utilization of dimensionality reduction and classification techniques. Specifically, Principal Component Analysis is employed for dimensionality reduction, while Weighted-K-nearest neighbors is utilized for appliance classification.

A. Dimensionality reduction

The common goal of PCA is to reduce high-dimensional data to lower dimensions while keeping most of the information by maximizing the variance of all projected samples. The TAR signature must be converted from a 2D matrix to a 1D vector in order to be used in PCA. This transformation is accomplished by concatenating the columns of the TAR signature. The process of PCA includes the first step, which is a training step, and another step, which is a testing step. The column vector of *M* samples represents the training set of the electrical load signature $\{a_1, a_2, a_3, \ldots\ldots, a_M\}$ in *n*-dimensional space. Eq. 5 can be utilized to calculate the mean of the training set.

$$\mu_a = \frac{1}{M}\sum_{j=1}^{M} a_j \qquad \text{(Eq. 5)}$$

The total scatter matrix or covariance matrix can be computed as :

$$G = \frac{1}{M}\sum_{j=1}^{M}(a_j - \mu_a)(a_j - \mu_a)^T \qquad \text{(Eq. 6)}$$

After finding the total scatter matrix, the goal of PCA is to find the eigenvector and eigenvalue of the covariance matrix. However, calculating eigenvectors directly can be computationally expensive and time-consuming. Therefore, the Singular Value Decomposition (SVD) approach is used to reduce computational complexities. As an outcome of the SVD computation, the needed eigenvector $U = [u_1, u_2, u_3, \dots, u_M]$ of G is produced, which corresponds to the eigenvalue $\alpha_1 \geq \alpha_2 \geq \alpha_3 \geq \dots \dots \geq \alpha_M$. In computing, the optimal eigenvectors U_{opt} are selected based on the cumulative sum of the P largest eigenvalues, where the index value P is determined as the lowest index value of the following percentage:

$$\frac{\sum_{j=1}^{P}\alpha_i}{\sum_{j=1}^{M}\alpha_j} \geq 95\% \qquad \text{(Eq. 7)}$$

The new j^{th} projected feature data b_j in the training set can be calculated from the sample a_j once the optimal eigenvector U_{opt} is determined. The projected feature data corresponding to the P-component of the eigenvector can be computed as follows:

$$b_j = U_{opt}^T(a_j - \mu_a) \qquad \text{(Eq. 8)}$$

It is less complicated throughout the testing procedure than during the training phase. Assume a' is an unknown input. Following the expression in (Eq. 9), the projected feature b' of the unknown input a' can be computed.

$$b' = U_{opt}^T(a' - \mu_a) \qquad \text{(Eq. 9)}$$

B. Appliance reconigtion

The low-dimensional subspace's projected feature is used as the input for an electrical load appliance belonging to one of the classes labeled in the dataset. To classify each type of appliance, one of the supervised learning algorithms called "Weighted k-Nearest Neighbors" is adopted to predict the unknown input type of electrical load appliance, where k is a number of neighbors and w is a weighted coefficient. This approach is rather simple by calculating the distance between unknown data b' and sample one b_j in the dataset and then selecting the k-nearest value of the sorted distance. The Euclidean distance is defined as:

$$D(b', b_j) = \|b' - b_j\| \qquad \text{(Eq. 10)}$$

The distance between unknown and sample data is represented as a matrix for each class of data. Then select the first k minimum distances. Finally, the class of unknown input can be predicted by following the class that has the maximum distance weight value determined as:

$$\underset{s \in C_s}{argmax} \sum_{j=1}^{k} w_j \delta(s, b_j) \qquad \text{(Eq. 11)}$$

where $w_j = \frac{1}{D^2(b', b_j)}$ is the weighted coefficient, and s is the class label.

C. Performance measure

The accuracy evaluation metrics are widely used for evaluating the classification procedure. To assess the performance of the proposed classification algorithm, various assessment measures such as accuracy, precision, recall, and F1-score are used. These metrics can be computed based on parameters of the confusion matrix, including True Positive (TP), True Negative (TN), False Positive (FP) and False Negative (FN), as described in Fig. 6.

Classification accuracy is defined as the ratio of correct predictions to total predictions. Precision, also known as positive predictive value, represents the number of correct positives predicted by the model in relation to the total number of positives predicted. Recall is also known as sensitivity or true positive rate. It is the positive rate between the predicted number of data points from our model and the actual number of data points. Precision and weighted harmonic recall are combined in the F1-socre [34].

		Predicted Classification			
	Classes	A	B	C	D
Actual Classification	A	TN	FP	TN	TN
	B	FN	TP	FN	FN
	C	TN	FP	TN	TN
	D	TN	FP	TN	TN

Fig. 6. Multi-class confusion matrix.

The performance assessment indication distinguishes the evaluation criteria to consider classification results with the elements of accuracy, f1-score, precision, and recall and can be formulated as:

$$Accuracy = \frac{TP+TN}{TP+TN+FP+FN} \quad \text{(Eq. 12)}$$

$$Precision = \frac{TP}{TP+FP} \quad \text{(Eq. 13)}$$

$$Recall = \frac{TP}{TP+FN} \quad \text{(Eq. 14)}$$

$$F-1\,Score = 2\left[\frac{Precision \times Recall}{Precision + Recall}\right] \quad \text{(Eq. 15)}$$

3. RESULTS AND DISCUSSION

This section presents the results of the simulations, followed by a comprehensive discussion and analysis of the findings to clear up the effectiveness and performance of the proposed algorithm in accurately identifying appliances. To evaluate the performance of the classification algorithm with the proposed multi-scale signatures, the PLAID datasets with three different versions are used. These datasets include both sub-metered and aggregated data. Only the sub-metered data is employed, which contains the voltage and current pairs sampled at 30 kHz of 1074 [35] and 1793 [36] individual appliances recorded from 11 different electrical home appliances and 1876 [37] from 16 different electrical home appliances in 2014, 2017, and 2020, respectively. Table 1 presents the number of samples of PlAID in three different versions.

Through 5-fold cross-validation, these sub-metered datasets are divided into training and testing sets in order to reach the best performance of the evaluated signature. The feature data is divided into five groups, which include training and testing sets. In each appliance class, 80% of the samples are utilized for training and the remaining 20% for testing.

Table 2 shows the performance of the classification algorithm for each dataset. The performance measures mentioned (accuracy, recall, F1 score, and precision) can be calculated through the expressions in (Eq. 12, Eq. 13, Eq. 14, and Eq. 15), which are frequently employed in machine learning and classification tasks. After the data is split into a training and testing set, the model is trained on the training data using the classification technique, then evaluated, and the prediction is made through the testing set. After obtaining the model's predictions for the testing set, we compare them with the true class label. It is important to emphasize that these performance measures were derived from experimental procedures and the evaluation of the model on an independent test dataset. Therefore, the results presented in Table 2 represent the comprehensive performance of five simulations conducted using a 5-fold cross-validation approach.

The result shows the W-KNN classifier on the PLAID of three different versions at the lowest *k*-nearest number (k = 1). According to the PLAID results, the 2017 version achieves the highest accuracy. This dataset obtained an accuracy of 97.43% (F1-Score of 96.98%), implying that it correctly classified 97.43% of all appliance samples. This indicates that the prediction has a relatively low rate of both false positives and false negatives. With a precision of 97.07% and a recall of 96.94%, the model demonstrates its successful ability to accurately identify the class of each appliance. In another version, specifically the 2014 version, an accuracy of 96.55% was achieved, along with an F1-score of 94.21%, recall of 94.32%, and precision of 94.25%. Additionally, in the year 2020, an accuracy of 97.13% was attained, accompanied by an F1-score of 90.88%, recall of 91.63%, and precision of 90.32%.

Table 3 presents the evaluation results for the PLAID dataset at different values of *k*. The results demonstrate the simulation's performance in terms of accuracy, precision, recall, and F1-score across the three versions. At k = 1, the result achieved remarkable accuracy scores: 96.55% for PLAID 2014, 97.43% for PLAID 2017, and an impressive 97.13% for PLAID 2020, indicating a high percentage of correct predictions. However, when *k* increased to 5, the accuracy scores decreased to 95.07% for PLAID 2014, 96.65% for PLAID 2017, and 95.48% for PLAID 2020. Furthermore, at k = 9, the accuracy scores further declined to 92.18% for PLAID 2014, 96.54% for PLAID 2017, and 92.44% for PLAID 2020.

Additionally, the highest precision, recall, and F1-score values were consistently observed at k = 1 across all three versions, showcasing the system's strong capability to accurately classify positive instances, effectively capture positive instances, and maintain a balanced precision-recall relationship, respectively.

Table 1 The sample number of PLAID with three different versions

PLAID	2014	2017	2020
Air conditioner	66	208	204
Blender			2
Coffee Maker			10
Compact fluorescent lamp	175	220	230
Fan	115	210	220
Fridge	38	90	108
Hair iron			10
Hair dryer	156	248	246
Heater	35	85	85
Incandescent light bulb	114	148	157
Laptop	172	207	216
Microwave	139	229	200
Soldering Iron			20
Vaccum	38	73	83
Washing Machine	26	75	75
Water Ketttle			10

Table 2 Performance measure with three versions of PLAID

PLAID	Accuracy	Precision	Recall	F1-Score
2014	96.55%	94.25%	94.32%	94.21%
2017	97.43%	97.07%	96.94%	96.98%
2020	97.13%	90.32%	91.63%	90.88%

Therefore, when we carefully compare the evaluation results for different values of k, we notice that there are slight decreases in accuracy, precision, recall, and F1-score for all versions of the PLAID dataset at k = 5 and k = 9. This suggests that increasing the value of k might lead to a slight degradation in performance. Figs. 7, 8, and 10 present the confusion matrices and showing the accuracy of each appliance corresponds to the various PLAID datasets.

It is observed that in Fig. 7, the predicted class is displayed in columns, while the true class is represented in rows. The diagonal elements represent the number of correctly predicted instances for each class. For instance, the model correctly predicted 58 Air conditioners, 173 compact fluorescents, and 115 Fans. Then, the sum of the values in a column excluding the diagonal element represents the instances that were incorrectly classified as belonging to that class. For example, the model incorrectly predicted 4 instances as Air conditioners when they actually belonged to other classes. Next, the sum of the values in a row excluding the diagonal element represents the instances of that class that were incorrectly classified as belonging to other classes. The model incorrectly predicted 2 instances of compact fluorescents as laptops.

Table 3 Performance evaluation of the PLAID dataset at different values of k

	Accuracy			Precision			Recall			F1-Score		
	k = 1	k = 5	k = 9	k = 1	k = 5	k = 9	k = 1	k = 5	k = 9	k = 1	k = 5	k = 9
2014	96.55%	95.07%	92.18%	94.25%	93.90%	91.06%	94.32%	92.16%	87.61%	94.21%	92.44%	88.61%
2017	97.43%	96.65%	96.54%	97.07%	95.74%	95.58%	96.94%	95.88%	95.73%	96.98%	95.76%	95.61%
2020	97.13%	95.48%	92.44%	90.32%	87.64%	85.22%	91.63%	89.69%	87.87%	90.88%	88.40%	86.17%

It can be observed that some appliances get 100% classification accuracy for each dataset, such as PLAID 2014 (3 appliances), PLAID 2017 (3 appliances), and PLAID 2020 (7 appliances). Vaccum gives an accuracy of 100% for versions 2017 and 2020. In both versions of 2014 and 2017, Fridge obtained classification accuracy of 73.7.% and 88.9%, respectively, which shows the lowest accuracy among all appliances in each dataset. In addition, this kind of load is always misclassified as Air conditioning and fans. It causes similar load signatures, making it challenging for the model to distinguish between them, but when the sample load data is increased, it also increases the accuracy. like Air conditioners and fans that have better performance than refrigerators.

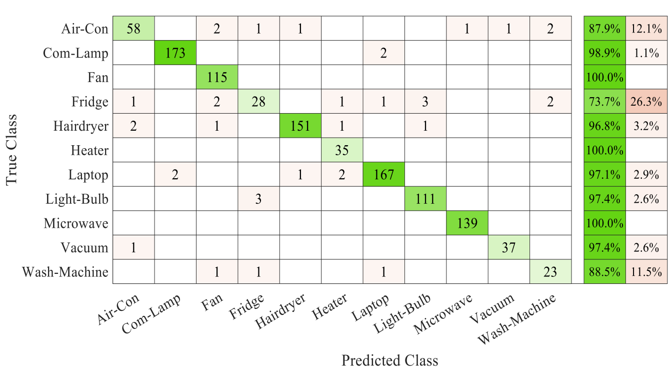

Fig. 7. Confusion matrix of weighted kNN for k =1 (PLAID 2014).

The observed similarity in the signatures of these four appliances, as depicted in the Fig. 9, implies that their V-I trajectories are closely aligned. Among these appliances, the fan stands out as an example. When the y-axis is expanded, it is highly probable that the fan's signature will resemble that of the other three figures, which exhibits a small size within the expanded range. Blender is 100% misclassified with Compact fluorescent lamp and Vaccum in PLAID 2020, as shown in Fig. 10.

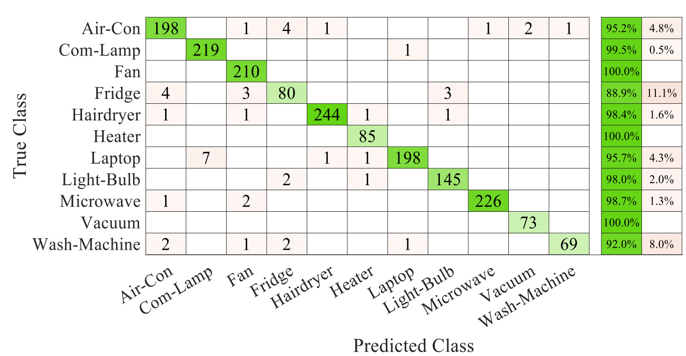

Fig. 8. Confusion matrix of weighted kNN for k =1 (PLAID 2017).

Due to the limited amount of training data available for a Blender, the model may not have learned enough patterns and features to accurately classify it. As previously discussed, 5-fold crossvalidation has been used to divide the training and testing sets. Additionally, since there are only two samples in the Blender overall sample, each fold should be randomly selected, with one sample serving as a training set and another as a testing set.

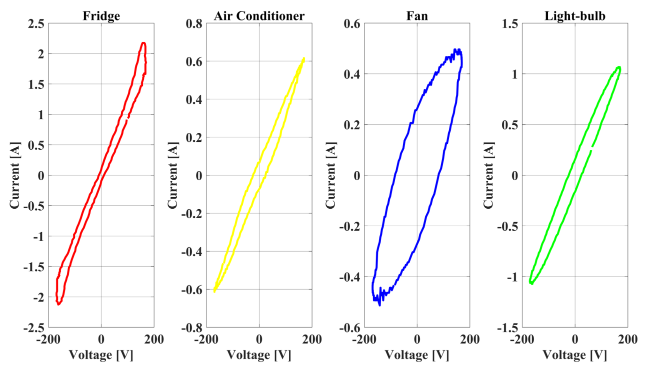

Fig. 9. V-I Trajectory load signatures of four different appliances: Fridge, Air Conditioner, Fan, and Light Bulb.

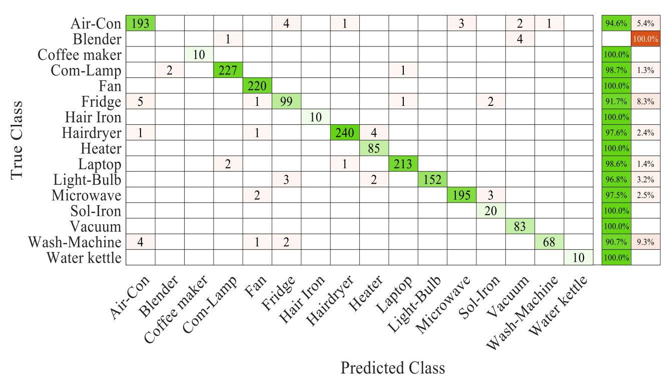

Fig. 10. Confusion matrix of weighted kNN for $k = 1$ (PLAID 2020).

Table 4. Comparison results on PLAID 2014 and 2017

	DCSS (RFC)		MTAR (W-KNN)	
	2014	2017	2014	2017
Accuracy	90.32%	85.67%	96.55%	97.43%
F1-score	86.14%	84.23%	94.21%	96.98%

Table 5. Accuracy comparison between the proposed classification algorithm and previous literature

Feature	Classifier	Accuracy
MTAR	W-KNN	97.43%
DCSS	RFC	85.67%
V-I, DCSS	RFC	84.72%
V-I, ECSS	2D-CNN	82.99%
Time series	RFC	80.70%

5. CONCLUSION

The paper presents a multi-scale signature as a representation for appliance load classification in Non-Intrusive Load Monitoring (NILM) systems. Specifically, a multi-scale V-I trajectory approach has been proposed to extract appliance load signatures. The proposed classification algorithm, which incorporates principal component analysis and weighted K-Nearest Neighbors, has been successfully validated for accurately recognizing load appliances. This approach effectively reduces high-dimensional data to a low-dimensional subspace, thereby improving the accuracy of load identification within the NILM classification framework. Consequently, it enables accurate identification and differentiation of various appliance types.

This study utilizes the V-I trajectory of one-cycle signals in steady-state regions, down-sampling them, and applying Fourier phase correction. The Triangle Area Representation (TAR) is used to represent the corrected starting point of each appliance's V-I trajectory, followed by dimensionality reduction using Principal Component Analysis (PCA). The low-dimensional feature is then classified using the Weighted K-Nearest Neighbors (W-KNN) algorithm. Evaluation with different versions of the PLAID dataset demonstrates the algorithm's accuracy, with the 2017 version performing the best. The multi-scale TAR signature with W-KNN achieves an accuracy of 97.43%, surpassing previous approaches. We have high accuracy, indicating that the model performs well overall. The precision and recall values are also high, indicating the model's successful ability to accurately identify the class of each appliance. The 2014 version achieved slightly lower accuracy but still performed well, while the 2020 version showed comparable accuracy but lower F1-Score, recall, and precision. The evaluation results highlight the effectiveness of using $k = 1$ in achieving the highest precision, recall, and F1-score values across all three versions of the PLAID dataset. These findings suggest that increasing the value of k may lead to a slight degradation in performance. Therefore, the optimal choice of k appears to be $k = 1$ for the most accurate and balanced classification results.

In our future work, the proposed approach will be implemented using our custom database. Furthermore, the scope of the research will be expanded by integrating additional steps, including the incorporation of event detection algorithms and the development of an energy disaggregation framework. The aim is to enhance the functionality and practicality of the NILM approach, with a specific focus on its application in real-time scenarios.

ACKNOWLEDGMENTS

The author would like to acknowledge Svay Rieng University for their support and funding under the High Education Improvement Project (HEIP).

REFERENCES

[1] Electricity Consumption by Country 2023. (n.d.) ElectricityConsumption by Country 2023.

[2] Gopinath, R., Kumar, M., Prakash Chandra Joshua, C., & Srinivas, K. (2020). Energy management using non-intrusive load monitoring techniques – State-of-the-art and future research directions. Sustainable Cities and Society, 62, 102411.

[3] Lin, Y. H., & Tsai, M. S. (2015). An Advanced Home Energy Management System Facilitated by Nonintrusive Load Monitoring With Automated Multiobjective Power Scheduling. IEEE Transactions on Smart Grid, 6(4), 1839–1851.

[4] Liu, H., Wu, H., & Yu, C. (2019, August). A hybrid model for appliance classification based on time series features. Energy and Buildings, 196, 112–123.

[5] Cambodia - Countries & Regions - IEA. (n.d.). IEA. https://www.iea.org/countries/cambodia

[6] Froehlich, J., Larson, E., Gupta, S., Cohn, G., Reynolds, M., & Patel, S. (2011). Disaggregated End-Use Energy Sensing for the Smart Grid. IEEE Pervasive Computing, 10(1), 28–39.

[7] Hart, G. (1989, June). Residential energy monitoring and computerized surveillance via utility power flows. IEEE Technology and Society Magazine, 8(2), 12–16.

[8] Zeifman, M., & Roth, K. (2011). Nonintrusive appliance load monitoring: Review and outlook. IEEE Transactions on Consumer Electronics, 57(1), 76–84.

[9] Drenker, S., & Kader, A. (1999). Nonintrusive monitoring of electric loads. IEEE Computer Applications in Power, 12(4), 47–51.

[10] Laughman, C., Kwangduk Lee, Cox, R., Shaw, S., Leeb, S., Norford, L., & Armstrong, P. (2003, March). Power signature analysis. IEEE Power and Energy Magazine, 1(2), 56–63.

[11] Chang, H. H., Lian, K. L., Su, Y. C., & Lee, W. J. (2014, May). Power-Spectrum-Based Wavelet Transform for Nonintrusive Demand Monitoring and Load Identification. IEEE Transactions on Industry Applications, 50(3), 2081–2089.

[12] Martins, J. F., Lopes, R., Lima, C., Romero-Cadaval, E., & Vinnikov, D. (2012, May). A novel nonintrusive load monitoring system based on the S-Transform. 2012 13th International Conference on Optimization of Electrical and Electronic Equipment (OPTIM).

[13] Sadeghianpourhamami, N., Ruyssinck, J., Deschrijver, D., Dhaene, T., & Develder, C. (2017, September). Comprehensive feature selection for appliance classification in NILM. Energy and Buildings, 151, 98–106.

[14] Zoha, A., Gluhak, A., Imran, M., & Rajasegarar, S. (2012, December 6). Non-Intrusive Load Monitoring Approaches for Disaggregated Energy Sensing: A Survey. Sensors, 12(12), 16838–16866.

[15] Kahl, M., Ul Haq, A., Kriechbaumer, T., & Jacobsen, H. A. (2017, May 16). A Comprehensive Feature Study for Appliance Recognition on High Frequency Energy Data. Proceedings of the Eighth International Conference on Future Energy Systems.

[16] Mulinari, B. M., Linhares, R. R., de Campos, D. P., da Costa, C. H., Ancelmo, H. C., Lazzaretti, A. E., Oroski, E., Lima, C. R. E., Renaux, D. P. B., & Pottker, F. (2019, September). A New Set of Steady-State and Transient Features for Power Signature Analysis Based on V-I Trajectory. 2019 IEEE PES Innovative Smart Grid Technologies Conference - Latin America (ISGT Latin America).

[17] Lam, H., Fung, G., & Lee, W. (2007). A Novel Method to Construct Taxonomy Electrical Appliances Based on Load Signaturesof. IEEE Transactions on Consumer Electronics, 53(2), 653–660.

[18] Hassan, T., Javed, F., & Arshad, N. (2014, March). An Empirical Investigation of V-I Trajectory Based Load Signatures for Non-Intrusive Load Monitoring. IEEE Transactions on Smart Grid, 5(2), 870–878.

[19] Wang, A. L., Chen, B. X., Wang, C. G., & Hua, D. (2018, April). Non-intrusive load monitoring algorithm based on features of V–I trajectory. Electric Power Systems Research, 157, 134–144.

[20] Thourn, K., Kitjaidure, Y., & Kondo, S. (2009). Eigen and Fisher Barycenter Contour for 2D Shape Classification. 2009 IEEE-RIVF International Conference on Computing and Communication Technologies.

[21] El Rube, I., Alajlan, N., Kamel, M., Ahmed, M., & Freeman, G. (2005). Efficient Multiscale Shape-Based Representation and Retrieval. Lecture Notes in Computer Science, 415–422.

[22] Jolliffe, I. T., & Cadima, J. (2016, April 13). Principal component analysis: a review and recent developments. Philosophical Transactions of the Royal Society A: Mathematical, Physical and Engineering Sciences, 374(2065), 20150202.

[23] Martinez, A., & Kak, A. (2001). PCA versus LDA. IEEE Transactions on Pattern Analysis and Machine Intelligence, 23(2), 228–233.

[24] Gao, J., Kara, E. C., Giri, S., & Berges, M. (2015, December). A feasibility study of automated plug-load identification from high-frequency measurements. 2015 IEEE Global Conference on Signal and Information Processing (GlobalSIP).

[25] Machlev, R., Tolkachov, D., Levron, Y., & Beck, Y. (2020, October). Dimension reduction for NILM classification based on principle component analysis. Electric Power Systems Research, 187, 106459.

[26] Moradzadeh, A., Sadeghian, O., Pourhossein, K., Mohammadi-Ivatloo, B., & Anvari-Moghaddam, A. (2020, April 14). Improving Residential Load Disaggregation for Sustainable Development of Energy

via Principal Component Analysis. Sustainability, 12(8), 3158.

[27] Chea, R., Thourn, K., & Chhorn, S. (2022, March 9). Improving V-I Trajectory Load Signature in NILM Approach. 2022 International Electrical Engineering Congress (IEECON).

[28] Du, L., He, D., Harley, R. G., & Habetler, T. G. (2016, January). Electric Load Classification by Binary Voltage–Current Trajectory Mapping. IEEE Transactions on Smart Grid, 7(1), 358–365.

[29] De Baets, L., Ruyssinck, J., Develder, C., Dhaene, T., & Deschrijver, D. (2018, January). Appliance classification using VI trajectories and convolutional neural networks. Energy and Buildings, 158, 32–36.

[30] Liu, Y., Wang, X., & You, W. (2019, September). Non-Intrusive Load Monitoring by Voltage–Current Trajectory Enabled Transfer Learning. IEEE Transactions on Smart Grid, 10(5), 5609–5619.

[31] De Paula Rodrigues, R., & da Silveira, P. M. (2021, January 2). Curvature scale space-based signatures for electrical load classification in NILM. Electrical Engineering, 103(2), 1239–1252.

[32] Bartolini, I., Ciaccia, P., & Patella, M. (2005, January). WARP: accurate retrieval of shapes using phase of Fourier descriptors and time warping distance. IEEE Transactions on Pattern Analysis and Machine Intelligence, 27(1), 142–147.

[33] Alajlan, N., El Rube, I., Kamel, M. S., & Freeman, G. (2007, July). Shape retrieval using triangle-area representation and dynamic space warping. Pattern Recognition, 40(7), 1911–1920.

[34] Grandini, M., Bagli, E., & Visani, G. (2020). Metrics for Multi-Class Classification: an Overview. ArXiv, abs/2008.05756.

[35] Gao, J., Giri, S., Kara, E. C., & Bergés, M. (2014, November 3). PLAID: a public dataset of high-resoultion electrical appliance measurements for load identification research. Proceedings of the 1st ACM Conference on Embedded Systems for Energy-Efficient Buildings.

[36] De Baets, L., Develder, C., Dhaene, T., Deschrijver, D., Gao, J., & Berges, M. (2017, December). Handling imbalance in an extended PLAID. 2017 Sustainable Internet and ICT for Sustainability (SustainIT).

[37] Medico, R., De Baets, L., Gao, J., Giri, S., Kara, E., Dhaene, T., Develder, C., Bergés, M., & Deschrijver, D. (2020, February 12). A voltage and current measurement dataset for plug load appliance identification in households. Scientific Data, 7(1).